International Journal of Biological Macromolecules 279 (2024) 135068

Contents lists available at ScienceDirect

International Journal of Biological Macromolecules

journal homepage: www.elsevier.com/locate/ijbiomac

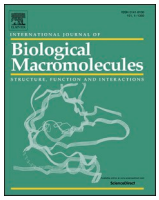

Supramolecular complexes of GCAP1: implications for inherited retinal dystrophies

Amedeo Biasi, Valerio Marino, Giuditta Dal Cortivo, Daniele Dell'Orco *

Department of Neurosciences, Biomedicine and Movement Sciences, Section of Biological Chemistry, University of Verona, 37134 Verona, Italy

ARTICLE INFO

Keywords:
RD3
Biologics
Guanylate cyclase

ABSTRACT

Guanylate Cyclase Activating Protein 1 (GCAP1) is a calcium sensor that regulates the enzymatic activity of retinal Guanylate Cyclase 1 (GC1) in photoreceptors in a Ca^{2+}/Mg^{2+} dependent manner. While point mutations in GCAP1 have been associated with inherited retinal dystrophies (IRDs), their impact on protein dimerization or on the possible interaction with the potent GC1 inhibitor RD3 (retinal degeneration protein 3) has never been investigated. Here, we integrate exhaustive *in silico* investigations with biochemical assays to evaluate the effects of the p.(E111V) substitution, associated with a severe form of IRD, on GCAP1 homo- and hetero-dimerization, and demonstrate that wild type (WT) GCAP1 directly interacts with RD3. Although inducing constitutive activation in GC1, the E111V substitution only slightly affects the dimerization of GCAP1. Both WT- and E111V-GCAP1 are predominantly monomeric in the absence of the GC1 target, however E111V-GCAP1 shows a stronger tendency to be monomeric in the Ca^{2+}-bound form, corresponding to GC1 inhibiting state. Reconstitution experiments performed in the co-presence of WT-GCAP1, E111V-GCAP1 and RD3 restored nearly physiological regulation of the GC1 enzymatic activity in terms of cGMP synthesis and Ca^{2+}-sensitivity, suggesting new scenarios for biologics-mediated treatment of GCAP1-associated IRDs.

1. Introduction

Visual perception is initiated by the phototransduction process in photoreceptors, a complex biochemical cascade which ultimately converts light absorption by visual pigments into cell membrane hyperpolarization, thus triggering the response of downstream neurons [1]. Phototransduction is finely regulated by the interplay between second messengers Ca^{2+} and cyclic guanosine monophosphate (cGMP), whose intracellular concentrations strictly depend on illumination. Indeed, photon detection by the G protein-coupled receptor (rhod)opsin results in the activation of phosphodiesterase 6, which hydrolyzes cGMP, thus causing the closure of cyclic nucleotide-gated (CNG) channels and a subsequent drop of the intracellular Ca^{2+}-concentration from several hundred nM in the dark to <150 nM in bright light [2]. Guanylate cyclase-activating proteins (GCAPs) are dimeric neuronal Ca^{2+}-sensor (NCS) proteins belonging to the EF-hand super family capable of detecting subtle changes in intracellular Ca^{2+}-concentration, thereby modulating the rate of cGMP synthesis in a Ca^{2+}-dependent fashion by interacting with retinal guanylate cyclases [3–5]. Of the three GCAP isoforms present in human rods and cones, namely GCAP1, GCAP2, and GCAP3, the former emerges as key regulator of Guanylate Cyclase 1 (GC1), the most relevant isozyme in the phototransduction cascade [6]. In the dark, high Ca^{2+} levels keep GCAP1 in a Ca^{2+}-bound state that inhibits GC1, preventing unnecessary cGMP synthesis; conversely, upon illumination Ca^{2+} levels fall, prompting GCAP1 to exchange Ca^{2+} for Mg^{2+} (Fig. 1A) and triggering a conformational change that stimulates GC1 activity and rapidly replenishes cGMP, which leads to the opening of CNG channels and, ultimately, the restoration of the Ca^{2+} concentration of the dark state.

Maintaining Ca^{2+} and cGMP homeostasis is imperative for both the viability and the functionality of photoreceptors, as more than twenty mutations in the *GUCA1A* gene (encoding for GCAP1) have been associated with inherited retinal dystrophies (IRDs), such as autosomal dominant cone (COD) and cone-rod (CORD) dystrophies [7–16], due to defective GC1 regulation. These disorders are characterized by progressive central vision loss, colour vision impairment, and altered sensitivity to light. The phenotypic heterogeneity observed in such dystrophies can be attributed to the specific amino acid substitutions,

* Corresponding author at: Department of Neurosciences, Biomedicine and Movement Sciences, Section of Biological Chemistry, University of Verona, Strada Le Grazie 8, 37134 Verona, Italy.
E-mail address: daniele.dellorco@univr.it (D. Dell'Orco).

https://doi.org/10.1016/j.ijbiomac.2024.135068
Received 7 June 2024; Received in revised form 16 August 2024; Accepted 23 August 2024
Available online 24 August 2024

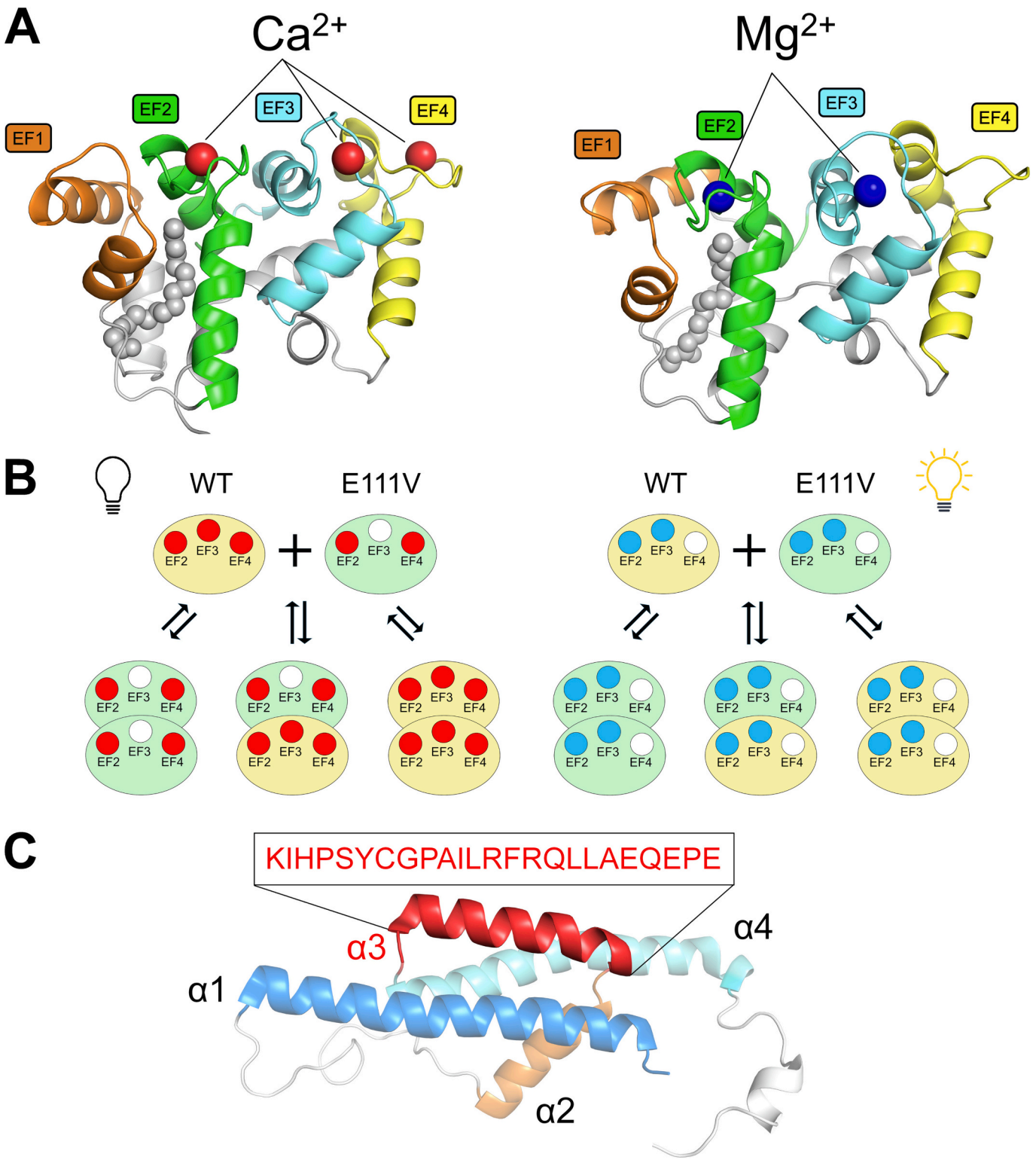

Fig. 1. (A) Cartoon representation of the three-dimensional homology model of monomeric Ca^{2+}-loaded (left) and Mg^{2+}-bound (right) human WT-GCAP1; EF1 is colored in orange, EF2 in green, EF3 in cyan and EF4 in yellow. N- and C-terminal are represented in light grey; Ca^{2+} and Mg^{2+} ions are shown as red and blue spheres, respectively, and the myristoyl group as grey spheres. (B) Schematic representation of the dimerization of WT- (yellow) and E111V-GCAP1 (green) in their GC1-inhibiting (left) and activating states (right), Ca^{2+} and Mg^{2+} ions are shown as red and blue circles, respectively, empty EF hands are shown as white circles. Equilibria leading to possible homo- and hetero-dimers are represented. (C) Cartoon representation of the three-dimensional structure of RD3 (PDB entry 6DRF [39]); helix α1 is colored in blue, helix α2 in orange, helix α3 in red and helix α4 in cyan. The sequence of helix α3 representing the RD3 peptide (RD3ppt) is reported.

each affecting the protein's ability to regulate GC1 differently, thereby disrupting the delicate second messenger equilibrium governing phototransduction. A variant of GCAP1, in which the bidentate coordinator glutamate 111 in the high-affinity Ca^{2+} − binding motif EF3 is replaced by a valine (E111V), leading to constitutive activation of GC1, was recently identified by some of us in a family affected by a severe form of CORD [14]. Constitutive activation of the GC1 target seems to be the common hallmark of all GCAP1-related IRDs [9,17], which all share autosomal dominant inheritance pattern. This makes the molecular scenario underlying GCAP1-associated IRDs especially intricate, as the protein is known to form dimers in a Mg^{2+}/Ca^{2+} dependent manner [3,18,19], which could result in a heterogeneous pool of homo- and heterodimers with unknown effects on GC1 regulation (Fig. 1B). Indeed, dimerization of GCAP1 has been suggested to affect its cellular compartmentalization and the regulation of the cyclase activity via allosteric mechanisms [20,21]. Another complication of the molecular scenario involving supramolecular complexes formed by GCAP1 is the yet unknown effect of the potential interaction between the IRD-associated GCAP1 variants and retinal degeneration protein 3 (RD3), a 23 kDa α-helical protein, recently emerged as a key factor in the preservation and functionality of photoreceptor cells [22,23]. With its submicromolar affinity, RD3 prevents GC1 premature activation within the photoreceptor's inner segment, thus averting potential cellular damage [24,25]. Indeed, RD3 mutations affecting its binding to GC1 or its inhibitory activity have been associated with Leber congenital amaurosis type 12 (LCA12) and CORD6 [26,27], while the lack of protein expression is associated with a marked decline of GC1 levels in photoreceptors outer segments and its accumulation in the inner segments, implicating a role for RD3 in the proper trafficking and localization of the cyclase [28–30]. RD3's pivotal inhibitory activity arises from specific surface-exposed residues essential for the interaction with GC1, which are either located in the coiled-coil domain between helices α1 and α2 or in helix α3 (Fig. 1C) [31].

This study explores the factors affecting the formation of GCAP1 supramolecular complexes both in the absence and in the presence of IRD-associated point mutations, focusing on the E111V variant, that we have previously characterized extensively from a clinical [14] and biomolecular viewpoint [32,33]. We used an integrated *in silico* and *in vitro* investigation approach to evaluate the functional consequences of the co-presence of a disease-associated point mutation and wild type (WT) GCAP1, as well as RD3 as a full protein or a peptide encompassing the region with stronger inhibitory capacity toward GC1. Besides shedding light on the basic mechanisms underlying GCAP1-mediated protein-protein interactions, our thorough investigation suggests conditions that could be exploited in the context of COD and CORD diseases to facilitate the re-establishment of the physiological homeostasis of cGMP and Ca^{2+}, with interesting applications for biologics-based therapeutics.

2. Materials and methods

2.1. Protein expression and purification

2.1.1. GCAP1 variants

The cDNA of human WT-GCAP1 (Uniprot entry: P43080) was purchased from Genscript and cloned into a pET-11a vector between *Nde*I and *Nhe*I restriction sites, while the E111V variant was introduced using QuikChange II Site-Directed Mutagenesis kit (Agilent) as detailed in [14]. Both variants were heterologously expressed in *E. coli* BL21(DE3) following co-transformation with pBB131 vector which contains the cDNA of *S. cerevisiae* N-myristoyltransferase (yNMT) necessary to achieve post-translational N-terminal myristoylation [34], and purified using the same protocol as previously detailed [14]. Briefly, proteins were purified from inclusion bodies after denaturation with 6 M guanidine-HCl, then underwent dialysis against 20 mM Tris-HCl pH 7.5, 150 mM NaCl, 7.2 mM β-mercaptoethanol buffer to allow refolding, and two sequential chromatographic steps, namely size exclusion chromatography (SEC, HiPrep 26/60 Sephacryl S-200 HR, GE Healthcare) and anion exchange chromatography (AEC, HiPrep Q HP 16/10, GE Healthcare). Protein concentration was measured by Bradford assay [35] using a GCAP1-specific reference curve based on the amino acid hydrolysis (Alphalyze), and its purity assessed on a 15 % SDS-PAGE gel. Finally, GCAP1 variants were exchanged against decalcified 50 mM NH_4HCO_3 buffer, flash-frozen in liquid nitrogen, lyophilized and stored at −80 °C until use.

2.1.2. RD3

The pETM-11-RD3 plasmid containing RD3 cDNA was a kind gift of Prof. K.W. Koch (Department of Neuroscience, Carl von Ossietzky Universität Oldenburg). RD3 was expressed in *E. coli* BL21(DE3) and purified by a series of centrifugation steps as previously reported [24]. Briefly, harvested cells were mechanically lysed with 3 sonication cycles on ice (30 s ON, 30 s OFF) and centrifuged at 4 °C at 10000 ×*g* for 10 min, then the insoluble fraction was washed 3 times against 10 mM Tris-HCl pH 7.5, 2 mM EDTA, 14 mM β-mercaptoethanol, 100 μM PMSF and 1× protein inhibitor cocktail (PIC), and centrifuged again at 4 °C at 15000 x g for 15 min. The insoluble fraction was denatured overnight using the same buffer with the addition of 8 M Urea, refolded by dialysis at 4 °C against 2 × 300 volumes (initial volume: 15 ml) of 10 mM Tris-HCl pH 7.5, 0.1 mM EDTA and 14 mM β-mercaptoethanol and centrifuged at 4 °C at 10000 ×*g* for 10 min. The supernatant containing RD3 was collected to assess protein purity via SDS PAGE and stored at −80 °C with 50 % v/v glycerol.

2.1.3. RD3 peptide

The RD3 peptide (RD3ppt), essential for the inhibitory activity of the protein [31], encompasses the region K87-E110 of RD3 corresponding to helix α3 (Fig. 1C), (sequence KIHPSYCGPAILRFRQLLAEQEPE) and was purchased by Genscript (purity >95 %, checked by HPLC). The lyophilized peptide was resuspended in pure bi-distilled water at a concentration of ~700 μM according to manufacturer instructions and stored at −80 °C until use.

2.2. Analytical size exclusion chromatography

The effects of the E111V mutation on GCAP1 dimerization under Ca^{2+} and Mg^{2+} concentrations mimicking the physiological signaling states were evaluated by analytical size exclusion chromatography (aSEC). Different GCAP1 concentrations (0.8 μM - 80 μM) were injected (200 μl) into a Superose 12 10/300 column (GE Healthcare) previously equilibrated with 20 mM Tris-HCl pH 7.5, 150 mM NaCl, 1 mM DTT, 1 mM Mg^{2+} buffer and either 0.5 mM EGTA or 0.5 mM Ca^{2+}. Elution profiles were collected by monitoring the absorbance at 280 nm, dissociation constants (K_{Dim}) for GCAP1 dimers were obtained by fitting the elution volume (V_e) to the concentration curve using Eq. (1) as in Ref. [18]:

$$V_e = A \bullet log\left(\left(\frac{[P_{TOT}] - \left(\frac{-K_{Dim}+\sqrt{K_{Dim}{}^2+4\bullet K_{Dim}\times[P_{TOT}]}}{2}\right)}{[P_{TOT}]}\right)\bullet 22.9 + 22.9\right) + B \quad (1)$$

where V_e represents the elution volume at the peak, A is the slope, $[P_{TOT}]$ is the concentration of the protein at the time of injection, B is the y-intercept and 22.9 is the monomer theoretical molecular mass (MM) of hGCAP1 in kDa. The MM of eluted samples was estimated using a calibration curve using cytochrome C (12.4 kDa), carbonic anhydrase (29 kDa), β-amylase (200 kDa) and alcohol dehydrogenase (150 kDa) as standards. Thus, the distribution coefficient D_c was calculated based on the V_e of the samples using Eq. (2):

$$D_c = \frac{(V_e - V_0)}{(V_i - V_0)} \quad (2)$$

where V_0 represents the void volume of the column (8.26 ml) and V_i is the total volume of the column (~ 24 ml). Ultimately, the MM of the samples was determined by plotting log(MM) vs D_c. Three replicates were performed for each condition (WT/E111V and Mg^{2+}/Ca^{2+}) and individually fitted according to the procedure described above.

2.3. Guanylate cyclase enzymatic activity assays

The effect of RD3ppt and RD3 on the regulation of GC1 activity by GCAP1 variants was investigated by performing enzymatic assays to monitor cGMP synthesis. Human recombinant GC1 was stably expressed in HEK293 cells after transfection with pcDNA3.1 + N-eGFP encoding for a fusion protein constituted by eGFP at the N-terminal and GC1 as previously described [33]. Membranes containing GC1 were isolated after cell lysis and resuspended in 50 mM HEPES pH 7.4, 50 mM KCl, 20 mM NaCl and 1 mM DTT. The inhibitory activity of RD3ppt was evaluated by incubating GC1 with 5 μM WT-GCAP1 and increasing concentrations of the peptide (0.05 μM - 15 μM) at low Ca^{2+} (< 73 nM). Minimum and maximum GC1 activities were determined by incubating GC1 with ~200 nM RD3 and WT- or E111V-GCAP1 or both to a final concentration of 5 μM, in the presence of high (~30 μM) or low Ca^{2+} (<19 nM). The effects of RD3 on GCAPs Ca^{2+} sensitivity (IC_{50}) were assessed by incubating GC1 with ~200 nM RD3 and either WT- or E111V-GCAP1 or their combination at a stoichiometric ratio of 3 WT-GCAP1: 1 E111V-GCAP1 to a final concentration of 5 μM in the presence of increasing free [Ca^{2+}] ranging from <19 nM to 1 mM. The GCAP1 concentration at which GC1 activation is half-maximal (EC_{50}) was estimated by incubating GC1 in the presence of <19 nM free Ca^{2+} with ~200 nM RD3 and increasing GCAP1 (WT, E111V or both) concentration from 0 to 15 μM. GC1 enzymatic reactions were performed in 30 mM MOPS/KOH pH 7.2, 60 mM KCl, 4 mM NaCl, 1 mM GTP, 3.5 mM $MgCl_2$, 0.3 mM ATP, 0.16 mM Zaprinast buffer and blocked with the addition of 50 mM EDTA and boiling at 95 °C. The synthesized cGMP was quantified by means of HPLC using a C18 reverse phase column (LiChrospher 100 RP-18, Merck). Data are reported as the mean ± standard deviation of at least three data sets.

2.4. Circular dichroism spectroscopy

Circular Dichroism (CD) spectroscopy in the far UV (200–250 nm) was employed to unveil alterations in secondary structure of GCAP1 upon RD3 binding under different ionic conditions. GCAP1 variants were resuspended in 20 mM Tris-HCl pH 7.5, 150 mM KCl, 1 mM DTT, while RD3 in 20 mM Tris-HCl pH 7.5, 1 mM DTT. Far-UV CD spectra of 10 μM RD3 were collected in the presence of 300 μM EGTA; while those of 10 μM GCAP1 were collected in the presence of 300 μM EGTA and after sequential additions of 10 μM RD3 and 600 μM Ca^{2+}, leading to approximately 300 μM free Ca^{2+}. Near-UV CD spectra of ~40 μM GCAP1 variants were collected in the presence of 500 μM EGTA and the addition of 1 mM $CaCl_2$, leading to 500 μM free Ca^{2+}. All CD spectra were recorded on a Jasco J-710 spectropolarimeter equipped with a Peltier-type cell holder in a 0.1-cm (1-cm for near UV experiments) path-length quartz cuvette with the following parameters: 1 nm bandwidth, 1 nm data pitch, 4 s integration time, 50 nm/min scanning speed, 25 °C temperature, 5 accumulations.

2.5. Molecular modelling

The three-dimensional structure of Ca^{2+}-loaded myristoylated human GCAP1 (UniProt entry: P43080), representing the GC1-inhibiting form, was obtained using the "Advanced Homology Modeling" tool provided by Bioluminate (Maestro package v. 12.5.139, Schroedinger) by selecting Ca^{2+}-loaded myristoylated GCAP1 from *G. gallus* (PDB entry: 2R2I [36]) as a template. The E111V substitution was introduced by *in silico* mutagenesis using Bioluminate "Mutate Residue" tool on the human structure by selecting the most likely rotamer for the sidechains. Mg^{2+}-bound GCAP1 variants, representing the GC1-activating form, were obtained by removing the Ca^{2+} ion attached to EF4 and replacing those in EF2 and EF3 with Mg^{2+}, as previously done [7,14,15,37,38]. Human RD3 structure displayed in Fig. 1 was obtained by selecting the first of the 10 conformers of human RD3 structure (PDB entry: 6DRF [39]).

2.6. Molecular dynamics simulations

Molecular Dynamics (MD) simulations of GCAP1 variants were performed on GROMACS 2020.3 package [40] using CHARMM36m [41] as the all-atom force field previously implemented with the parameters for the N-terminal myristoylated Gly (available on request). Two-step energy minimization and equilibration (2 ns in NVT ensemble with and without position restraints) were carried out as previously described [38]. For each state, namely Ca^{2+}-loaded WT- and E111V-GCAP1 (Ca^{2+}-ions bound to EF2, EF3 and EF4), Ca^{2+}-bound E111V-GCAP1 (Ca^{2+}-ions bound to EF2 and EF4), and Mg^{2+}-bound WT- and E111V-GCAP1 (Mg^{2+}-ions bound to EF2 and EF3) four independent 1 μs trajectories at constant pressure (1 atm) and temperature (310 K) were produced. The exhaustiveness and consistency of the trajectories was assessed by means of Principal Component Analysis (PCA) of the Cα (representing the largest collective motion of the protein), Linear Discriminant Analysis (LDA) on the first two principal components, and Root-Mean Square Inner Product (RMSIP) of the first twenty principal components following a previously detailed pipeline [38]. Once their reproducibility was assessed for each state, the four trajectories were concatenated and the flexibility of the proteins was investigated by means of Root-Mean Square Fluctuation (RMSF) of the Cα, which represents the residue-specific time-averaged Root-Mean Square Deviation (RMSD) calculated with respect to the average positions along the 4 μs trajectories. Analogously, the RMSF of ions bound to individual EF-hands was calculated to evaluate the mobility of the ions within the loop, indicative of potential alterations of the optimal geometry required for ion coordination. In the case of Ca^{2+}-loaded E111V-GCAP1, the RMSF was also calculated only on the three replicas in which the ion did not dissociate to exclude potential artifacts due to ion diffusion.

2.7. Molecular docking simulations

The centroid of the conformations sampled by the 4 μs MD simulations of GCAP1 variants were used as ligand and receptor for protein-protein rigid-body docking simulations of GCAP1 dimers using ZDOCK 3.0.2 [42], which comprised 4 independent docking runs per tested case with a sampling step of 6° (dense sampling) starting from different relative orientations, each resulting in 4000 complexes. Docked poses were filtered by selecting structurally analogous conformations exhibiting a Cα RMSD < 1 Å with respect to the reference complex structure representing the highest-scored dimer described in ref. [18] using the same criterion as in [43,44]. The average ZDOCK score of the filtered solutions (ZD-s) was used to estimate the free energy of binding (ΔG°) based on their correlation with experimental data [43,44].

2.8. Surface plasmon resonance

Surface plasmon resonance (SPR) experiments were conducted using a SensiQ Pioneer apparatus and a COOH1 sensor chip (Sartorius) presenting a low-capacity two-dimensional surface chemistry that comprises a polyethylene glycol spacer terminated with carboxylic acids, which is particularly suitable for large molecule kinetic analysis. The chip was preconditioned according to the manufacturer protocol, consisting of 2 cycles of sequential injections of 25 μl HCl 0.1 M, 25 μl NaOH 50 mM, 25 μl SDS 0.5 %, and 25 μl EDTA 0.3 M at 100 25 μl/min

flowrate. RD3 was covalently immobilized on the sensor chip via the site-specific thiol-disulfide exchange strategy. Briefly, the surface of the sensor chip was activated with an injection of 70 μl mixture of 50 mM N-hydroxysuccinimide (NHS) and 200 mM N-ethyl-N′-(dimethylaminopropyl)-carbodiimide (EDC) at 5 μl/min, followed by a 70 μl injection of 80 mM 2-(2-pyridinyldithio)ethaneamine hydrochloride (PDEA) in 0.1 M sodium borate buffer (pH 8.5), at 5 μl/min. RD3 was exchanged against bi-distilled water, diluted to 10 μM in 10 mM sodium acetate buffer (pH 4.3) and immobilized by thiol-disulfide exchange upon injection of 200 μl at 5 μl/min. After immobilizing ~700 RU, the remaining thiol groups on the chip surface were inactivated by injecting 50 μl of a mixture of 50 mM L-cysteine and 1 M NaCl in 10 mM sodium acetate buffer (pH 4.0) at 5 μl/min.

The protocol for monitoring GCAP1 variants binding to immobilized RD3 consisted in injections of 200 μl of 1 μM, 2 μM and 5 μM GCAP1 variants (dissolved in 10 mM HEPES, 150 mM NaCl, 300 μM Ca^{2+}, 0.005 % Tween 20, pH 7.4) at 20 μl/min, with a dissociation time of 600 s. To avoid artifacts deriving from the ageing of the sensor chip surface, GCAP1 variants were assayed alternately (3 injections for WT- followed by 3 injections for E111V-GCAP1) and the protocols were repeated 4 times, for a total of 12 injections for each variant. The dissociation phase was fitted according to a first-order reaction, using the following exponential decay model to estimate the dissociation rate constant:

$$RU(t) = RU_0 \bullet e^{-k^{off} \bullet t} \quad (3)$$

where RU_0 is the maximum signal at each specific concentration and k^{off} is the dissociation rate constant, which was calculated for WT-GCAP1 as average ± standard error of the mean of 10 injections. The association phase was fitted by a pseudo-first order model according to this equation:

$$RU(t) = \frac{k^{on} R_{max}[GCAP1]}{k^{on}[GCAP1] + k^{off}} \left(1 - e^{-\left(k^{on}[GCAP1] + k^{off}\right)t}\right) + R_0 \quad (4)$$

where R_0 is the baseline, R_{max} is the maximum SPR response that would be expected if all the active immobilized RD3 molecules would interact with GCAP1 and [GCAP1] is the analyte concentration at each injection, while k^{on} is the association rate constant, obtained as average ± standard error of the mean of 9 injections. The affinity of GCAP1 for RD3, in μM, was calculated in terms of dissociation equilibrium constant: $K_D = k^{off}/k^{on}$.

3. Results and discussion

To dissect the formation of the supramolecular complexes involving GCAP1-GC1 and potentially RD3, and to evaluate the putative role of the E111V point mutation, we applied a stepwise procedure, which started from the computational characterization of GCAP1 monomers in the possible signaling states (Fig. 1B). Exhaustive, 4 microsecond MD simulations formed the basis for studying the stability of the protein and the allosteric mechanisms arising from the specific ligand and/or mutated state; moreover, the output of MD simulations was used to build a reliable structural model of the GCAP1 dimer using protein-protein docking, which permitted direct comparisons with experimental results from analytical size exclusion chromatography. Finally, we tested whether RD3, both in a shorter form via a peptide encompassing helix α3, or in the full-length version, was able to interact with GCAP1 as well as with GC1, and exert a controlled inhibition of the cyclase in the presence of WT- and E111V-GCAP1. The results are summarized in the following paragraphs.

3.1. Conformational properties of WT/E111V-GCAP1 monomers: molecular dynamics simulations suggest increased structural flexibility for E111V-GCAP1

Previous works highlighted that the E111V substitution, in which an acidic glutamate residue involved in the coordination of Ca^{2+} is replaced by the hydrophobic valine, only slightly affects secondary and tertiary structure of GCAP1 [14,33] while dramatically impairing the affinity for Ca^{2+} and preventing the binding of the cation to EF3. The altered affinity for Ca^{2+} reflects on the dysregulation of GC1 activity and leads to its constitutive activation. In the present study, we investigated at atomistic resolution the molecular determinants underlying ion binding to GCAP1 variants by running 4 μs MD simulations of the protein under GC1-activating (Mg^{2+} bound to EF2 and EF3 in both variants) and GC1-inhibiting conditions (Ca^{2+} bound to EF2, EF3 and EF4 in both variants, and bound only to EF2 and EF4 for the E111V substitution).

In line with previous spectroscopic data [14,33], exhaustive MD simulations revealed a significant distortion of the EF3 loop of the E111V variant compared to the WT, which significantly destabilized the coordination of Ca^{2+} in EF3 (Fig. 2A). On the other hand, no significant structural rearrangement was observed throughout the trajectory, although the RMSF profiles highlighted a significantly higher backbone flexibility for E111V-GCAP1 bound to 2 or 3 Ca^{2+} ions compared to the WT, especially in the region corresponding to EF3 (Fig. 2B); this is not surprising, since the mutated residue is located in that EF-hand motif, thus pointing to a local structural perturbation. Interestingly, this reflected not only in a significantly higher fluctuation of the Ca^{2+}-ion in EF3 (138.2 Å for 3Ca-E111V vs 1.01 for 3Ca-WT-GCAP1, Supplementary Table ST1), which spontaneously dissociated in one of the replicas (RMSF = 3.29 Å excluding such replica), but also in EF4 (3.27 Å for 3Ca-E111V and 1.63 Å for 2Ca-E111V vs 1.23 Å for 3Ca-WT-GCAP1, Supplementary Table ST1) and, to a lesser extent, in EF2 (2.02 Å for 3Ca-E111V and 2.04 Å for 2Ca-E111V vs 1.1 Å for 3Ca-WT-GCAP1, Supplementary Table ST1), suggesting an allosteric effect of the mutation, which was already pointed out in shorter simulations [38]. As to the Mg^{2+}-bound forms, the E111V substitution displayed minor differences with the WT both in terms of backbone flexibility (Fig. 2C) and in ion coordination, as shown by the comparable RMSF of Mg^{2+}-ions in EF2 (1.30 Å vs 1.23 Å, Supplementary Table ST1) and EF3 (2.2 Å vs 1.9 Å, Supplementary Table ST1), thus suggesting that the GC1-activating state does not change significantly from the structural viewpoint between IRD-associated and WT condition, at least as far as isolated structures of GCAP1 monomers are concerned. This result is also in line with previous spectroscopic characterizations by us based on near UV CD spectroscopy [14,33].

3.2. In silico dimerization of WT- and E111V-GCAP1 suggests very similar binding modes

The similar structural features of WT- and E111V-GCAP1 monomers suggest that they might dimerize in a comparable manner, although this process was not explicitly investigated yet. The Ca^{2+}- and Mg^{2+}-dependent dimerization of GCAP1 could play a role in the phototransduction cascade, for example affecting the binding to, and therefore the regulation of the GC1 target [3,45]. The complexity of the molecular scenario is increased in the presence of IRDs, as the autosomal dominant inheritance pattern of mutations associated with COD and CORD suggests that, in the outer segments of photoreceptors under these conditions, a pool of homo- and heterodimers might be present. To test whether and how the presence of the E111V mutation in well-defined signaling states can affect protein dimerization, we used an *in silico* approach based on rigid-body docking, which led to the reconstitution of potential dimeric assemblies of GCAP1 (WT/WT, E111V/E111V, WT/E111V) under the same cation-bound conditions used in MD simulations (see Section 3.1). In order to discriminate the poses obtained by docking protein monomers, we considered as “native like” the highest-scored assembly that was previously validated by small-angle X-ray scattering (SAXS) data [18], characterized by specific hydrophobic contacts at the GCAP1 dimer interface. In particular, dimer formation is driven by the interaction between residues located on αE1 and αF2 from one monomer and amino acids on αE1, αF2 and αE3 from the second monomer [18].

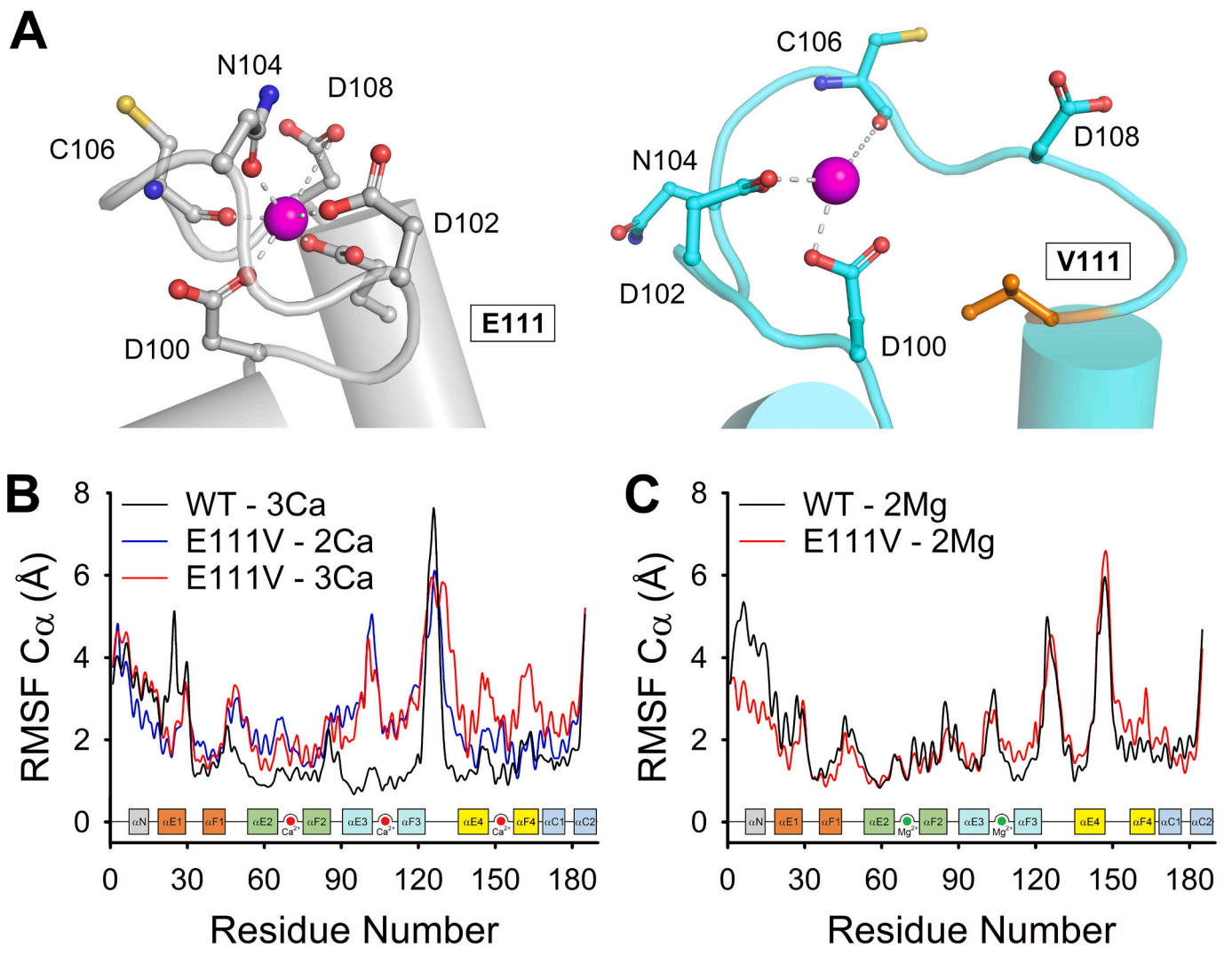

Fig. 2. Results from exhaustive 4 μs MD simulations. (A) Representative Ca^{2+}-coordination in EF3 of WT-GCAP1 (left) and E111V-GCAP1 (right) after 1 μs MD simulations. WT-GCAP1 and E111V-GCAP1 structures are shown as grey and cyan cartoon, respectively; Ca^{2+}-coordinating residues are labelled and represented as sticks with C atoms in the same colour as the structure, O atoms in red, N atoms in blue and S atoms in yellow; Ca^{2+} ions are shown as purple spheres; CORD-associated V111 is shown as orange sticks. (B) Cα-RMSF of WT-GCAP1 bound to 3 Ca^{2+} ions (black), E111V-GCAP1 with ions bound in EF2 and EF4 (blue), and E111V-GCAP1 bound to Ca^{2+} ions (red). (C) Cα-RMSF of WT-GCAP1 (black) and E111V-GCAP1 (red) with Mg^{2+} ions bound to EF2 and EF3. Insets show the secondary structure elements colored according to Fig. 1A and the position of ion-binding loops.

Table 1
Results from Rigid-Body Docking simulations of GCAP1 dimers and from analytical SEC experiments.

Assembly	Ions	Native-like poses[a]	RMSD[b] (Å)	ZD-s[c]	Best ranked[d]	ΔG° [e] (kcal/mol)	ΔΔG° [f] (kcal/mol)	K_{Dim}[g] (μM)
WT-WT	3Ca	22	0.85 ± 0.1	54.4 ± 0.8	1	−17.36	–	12.0 ± 0.8
	2Mg	22	0.84 ± 0.1	54.0 ± 0.8	1	−17.20	–	6.1 ± 3.3
WT-E111V	2Ca	21	0.86 ± 0.1	54.6 ± 0.8	1	−17.41	−0.06	
	3Ca	21	0.86 ± 0.1	54.8 ± 0.8	1	−17.50	−0.14	–
	2Mg	21	0.85 ± 0.1	54.3 ± 0.8	1	−17.32	−0.12	
E111V-E111V	2Ca	18	0.84 ± 0.1	54.5 ± 0.9	1	−17.39	−0.04	16.7 ± 3.2
	3Ca	18	0.84 ± 0.1	54.9 ± 0.9	1	−17.55	−0.20	
	2Mg	18	0.84 ± 0.1	54.4 ± 0.9	1	−17.36	−0.16	4.2 ± 3.4

[a] Number of docked complexes with Cα-RMSD <1 Å with respect to the experimentally validated dimeric model [18].
[b] Average RMSD of the native-like poses.
[c] Average ZDOCK score (ZD-s) of native-like poses ± standard deviation.
[d] Rank of the best native-like pose out of the total 16,000 proposed.
[e] Gibbs free energy of binding.
[f] Difference in Gibbs free energy of binding calculated with respect to WT dimers.
[g] Dimerization constant obtained by analytical SEC presented as average ± standard deviation of three technical replicates.

For all tested conditions, docking simulations predicted a comparable number of native-like poses, ranging from 18 to 22 in the case of the E111V and WT homodimer, respectively (Table 1), with average RMSD compared to the reference structure spanning between 0.84 ± 0.1 and 0.86 ± 0.1 Å, Table 1). Interestingly, the highest-scored pose out of the 16,000 complexes outputted by ZDOCK (Table 1) was always selected as a native-like pose, thus implying that the assembly of both WT- and E111V-GCAP1 is essentially compatible with that previously validated by SAXS data, and that the binding may indeed occur in an essentially rigid body-like manner. On the same line, the average ZD-s of the native-like solutions in all conditions tested ranged between 54.0 ± 0.8 and 54.9 ± 0.9 in the case of Mg^{2+}-bound WT homodimer and 3 Ca^{2+}-bound E111V, respectively. Moreover, all comparisons between the average ZD-s of GCAP1 dimers representing the same signaling state (WT-WT 3Ca vs WT-E111V/E111V-E111V 2Ca/3Ca and WT-WT 2 Mg vs WT-E111V/E111V-E111V 2 Mg) by means of two-tailed *t*-tests (*p*-value = 0.05) were found not to be significant. The average ZD-s can be used to empirically derive the free energy of dimerization, provided that the binding occurs without major conformational changes [43,44]. The predicted ΔG° values (ranging between −17.22 and − 17.55 kcal/mol (Table 1) were all very similar to each other, despite the different conditions. Indeed, by inferring state- and variant-specific changes in the free energy of binding (ΔΔG°), docking results highlighted only subtle differences in binding affinities (< −0.2 kcal/mol, Table 1), which were more pronounced when residue V111 was involved in ion binding, that is in the case of 3Ca and 2Mg (Table 1). Overall, these *in silico* results suggest that the WT and the E111V variants dimerize with very similar quaternary structure and affinity.

3.3. *In vitro dimerization of GCAP1 variants suggests higher propensity to dimerize in the Mg^{2+}-bound form*

Since rigid-body docking simulations predicted neglectable differences in binding affinities upon homo- and heterodimer formation in the presence of either Ca^{2+} or Mg^{2+} ions, the propensity of GCAP1 variants to form dimers under different ion-loading conditions was validated *in vitro* by injecting decreasing concentrations (80 μM – 0.8 μM) of GCAP1 in an analytical SEC column and comparing the elution volume with that of 4 reference proteins. In the presence of Ca^{2+}, the estimated MM of WT-GCAP1 injected at 80 μM was ~41 kDa, thus compatible with a dimer, with a concentration at the elution peak calculated from the absorbance at 280 nm of ~16 μM (MM/ε = 1.07 mg/ml). Injections at lower concentrations resulted in a peak shift toward higher elution volume, hence lower apparent MM, confirming the presence of a monomer-dimer equilibrium. The analysis of elution profiles (Fig. 3), based on the relationship between the elution volume and the molecular mass of the complex (which depends on the equilibrium constant for GCAP1 dimerization), and the concentration at the peak, led to the estimated equilibrium constants for GCAP1 dimerization reported in Table 1. An overall agreement with *in silico* docking experiments could be noted in terms of similar binding modes of WT- and E111V-GCAP1, regardless of the mutation and the specific signaling state; however, analytical SEC permitted higher precision in determining the binding affinities, which are not affected by the requirement of rigid body-like interaction. Interestingly, a slightly reduced dimer affinity was detected for E111V-GCAP1 in the presence of Ca^{2+} compared to the WT (K_{Dim}^{E111V} = 16.7 ± 3.2 μM vs K_{Dim}^{WT} = 12.0 ± 0.8 μM), while the slight increase in affinity exhibited by the Mg^{2+}-bound forms compared to the

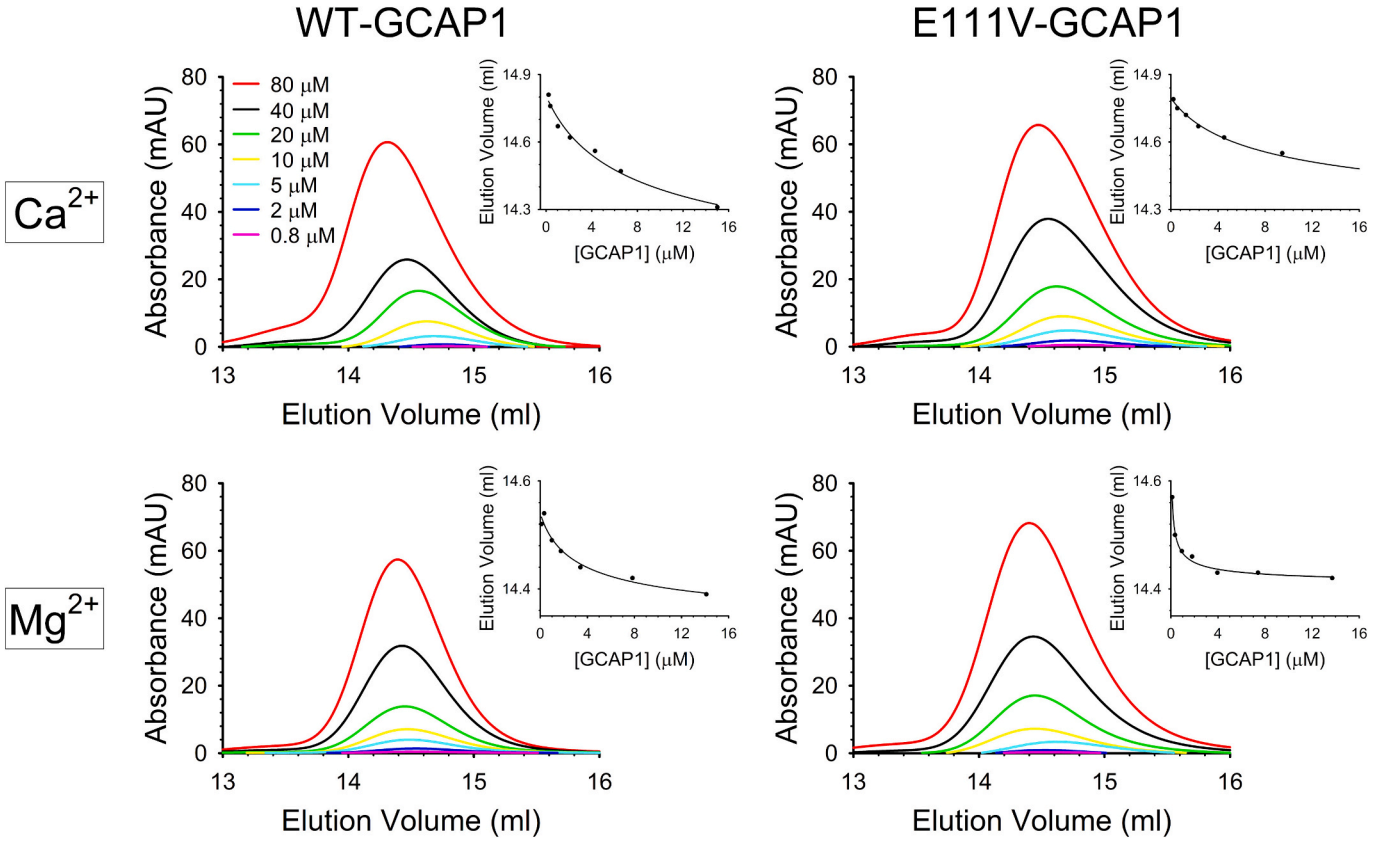

Fig. 3. Representative analytical SEC chromatograms of 80 μM (red), 40 μM (black), 20 μM (green), 10 μM (yellow), 5 μM (cyan), 2 μM (blue), and 0.8 μM WT-GCAP1 (left panels) or E111V-GCAP1 (right panels) in the presence of 1 mM Mg^{2+} and 0.5 mM Ca^{2+} (upper panels) or 0.5 mM EGTA and 1 mM Mg^{2+} (lower panels). Insets show the elution volume as a function of the protein concentration estimated from the absorbance at the chromatographic peak, together with the theoretical fitting curve (Eq. (1)) detailed in Section 2.2. Three technical replicates were performed for each condition and independently fitted to Eq. (1), the estimated equilibrium constants for the dimerization process are reported in Table 1 as mean ± standard deviation.

WT ($K_{Dim}^{E111V} = 4.2 \pm 3.4$ μM vs $K_{Dim}^{WT} = 6.1 \pm 3.3$ μM) was within the error bars, so not significant. However, when the comparison was done for each variant, looking at the Ca^{2+} vs. Mg^{2+}-bound forms, the increase in the tendency to dimerize in the Mg^{2+}-bound form was much higher for the E111V variant (~4-fold) than for the WT (~2-fold). These findings diverge from previously obtained results in which WT-GCAP1 binding affinity decreases switching from a Ca^{2+} ($K_{Dim}^{WT} = 8.8 \pm 0.7$ μM) to a Mg^{2+}-bound state ($K_{Dim}^{WT} = 45 \pm 15$ μM) [18]. The discrepancies can be attributed to a different ionic strength of the aSEC buffer (100 mM vs 150 mM NaCl), its pH (8.0 vs 7.5) and a much higher concentration of free Mg^{2+} (~4 mM vs ~0.9 mM) which altogether represent a less physiological environment if compared to the experimental parameters presented in this work. Overall, these results suggest that the IRD-associated variant has stronger tendency to be monomeric in the Ca^{2+}-bound form, corresponding to GC1 inhibiting state, and to dimerize in the absence of Ca^{2+}, that is in the GC1-activating form. If dimerization of GCAP1 was a requirement for GC1 activation, this result could partly explain the variant's tendency to induce constitutive activation in the target enzyme.

Previous results on the V77E-GCAP1 variant, which was shown to abolish protein dimerization, showed that also the GC1 activation was seriously compromised [20,21], which would support a mechanism that requires GCAP1 dimerization for the correct activation of GC1. On the other hand, it should be noted that, if the same cellular concentration of GCAP1 measured in bovine rods (3.3 μM [46]) is assumed to be valid for human photoreceptors, our estimated K_{Dim} values would point to the two isolated variants being predominantly monomers under Ca^{2+}-saturating conditions (75.5 % and 78.8 % for WT- and E111V-GCAP1, respectively) and, to a lesser extent, in the Mg^{2+} − bound form (66.7 % and 61.2 % for WT- and E111V-GCAP1, respectively). It remains therefore essential to establish whether GCAP1 dimerization is facilitated by the interaction with the GC1 target, and if dimerization is a prerequisite for its activation.

3.4. *Using RD3-induced inhibition of GC1 to probe novel therapeutic hypotheses for IRD in the presence of E111V-GCAP1*

The modulation of GC1 activity is a fundamental step in phototransduction, to ensure physiological response and photoreceptor viability. We previously demonstrated *in vitro* that WT-GCAP1 significantly attenuates the dysregulation of GC1 induced by E111V-GCAP1 [32] and that direct retinal delivery of the mutated protein in a WT mouse induces a disease-phenotype [33]. Although the delivery of extra WT-GCAP1 was shown to partly restore the Ca^{2+} sensitivity of GC1, numerical simulations suggest that this amelioration is not enough to fully prevent retinal degeneration, as the levels of Ca^{2+} and cGMP would remain higher than normal [32]. These preliminary data nonetheless suggest that the combination of WT-GCAP1 and GC1 inhibitors could be a promising avenue for addressing the dysregulated cGMP production implicated in IRDs in the presence of variants such as E111V-GCAP1. In this study we probed whether the potent GC1-inhibitor RD3 could contribute to this effective combination. We therefore tested the effects on GC1 regulation by WT- and E111V-GCAP1 variants of RD3 as a full-length protein as well as a peptide (named RD3ppt) corresponding to the interacting helix α3 (Fig. 1C), which was described as a fundamental component for achieving high inhibiting capacity of the cyclase [27].

The GC1 activity at increasing amounts of RD3ppt in the 50 nM - 15 μM range suggested a dose-dependent partial inhibition of either WT- or E111V-GCAP1 (Fig. S4A) mediated regulation, at least up to 5 μM. However, the errors associated with each data point did not allow a reliable estimation of the IC_{50} or a quantitative comparison of the effects on WT and E111V variants. On the other hand, full-length RD3 showed significatively enhanced inhibitory efficacy of the WT-GCAP1-GC1 complex (Fig. S4B), with an IC_{50} of 68.4 ± 4.9 nM. This high inhibition capability of RD3 is in line with previous observations [27,30,47] and could be used as a further element to attenuate the dysregulation of GC1 induced by E111V-GCAP1 [32].

Although it has been established that RD3 interacts with GC1 to promote its correct targeting to the photoreceptor outer segment, the interaction between RD3 and GCAP1 is thought to constitute a functional requirement to properly achieve such targeting; indeed, *in vivo* studies suggested that disrupting the GC1-GCAP1 and RD3 complex in the endoplasmic reticulum is associated with Leber congenital amaurosis 1 [30]. Despite the strong evidence of interaction by *in cyto* and *ex vivo* imaging, the interplay between RD3 and GCAP1 is still poorly understood. We have hence investigated by CD spectroscopy the interaction between GCAP1 variants and RD3, to possibly elucidate the molecular fingerprints defining the RD3-GCAP1 complex.

The far UV CD spectrum of Mg^{2+}-bound WT-GCAP1 exhibited, as expected, the spectrum of a typical all α-helical protein with minima at 208 and 222 nm, similarly to full-length RD3 (Fig. 4A-B). In addition, both WT- and E111V-GCAP1 variants exhibited a minor increase in ellipticity upon switching from the Mg^{2+}-bound form to the Ca^{2+}-bound form (3 % and 2.6 % for WT- and E111V-GCAP1, respectively, Fig. 4A-B, Table 2). Such increase in ellipticity was accompanied by a change in spectral shape in the case of WT-GCAP1 ($\theta_{222}/\theta_{208} = 0.89$ vs 0.92, Table 2), while that of E111V was almost negligible ($\theta_{222}/\theta_{208} = 0.89$ vs 0.90, Table 2). The potential interaction between RD3 and GCAP1 variants was assessed by comparing the spectrum of the putative complex with that of the sum of the isolated proteins; the fact that the spectrum obtained when incubating the protein and the peptide differed from to the sum of those of the individual proteins should indicate an interaction between the two macromolecules. Interaction was detected for full-length RD3 upon incubation with Mg^{2+}-bound GCAP1 variants (Fig. 4D-E), as shown by the almost halved signal compared to the theoretical sum of the spectra.

To further investigate the interaction between GCAP1 variants and RD3 we performed Surface Plasmon Resonance (SPR) experiments by flowing GCAP1 variants onto RD3, which was previously site-specifically immobilized on the sensor chip surface by thiol-disulfide exchange. Interestingly, the two GCAP1 variants exhibited a completely opposite behavior. At odds with WT-GCAP1, no binding curves could be identified for E111V-GCAP1 regardless of the injected concentration (Fig. 5A and B), although both proteins were verified to be correctly folded and functional by means of near UV CD spectroscopy (Fig. 5C and D). This suggests that the differences in secondary structure in the presence of RD3 and GCAP1 variants observed in the far UV CD spectra may rise from different molecular mechanisms.

Interestingly, the interaction between WT-GCAP1 and RD3 could be well described by a simple 1:1 Langmuir model (Fig. 5A), yielding a dissociation rate constant (k^{off}) of (5.1 ± 0.3) x 10^{-3} s^{-1}, which corresponds to a complex half-time ($t_{1/2}$) of ~136 s, indicative of a relatively stable complex for a protein-protein interaction involved in signaling events. The association process was not particularly fast, resulting in an association rate constant (k^{on}) of (1.9 ± 0.6) x 10^3 M^{-1} s^{-1}. The kinetic parameters are consistent with an affinity for the GCAP1-RD3 complex (K_D) of 2.7 ± 0.9 μM, thus comparable to the apparent affinity of GCAP1 for GC1 (see EC_{50} values reported in Table 3), suggesting the possible co-existence of GCAP1-RD3-GC1 dynamic complexes, as already suggested by *Zulliger et al.* [30].

Once verified the direct interaction between RD3 and GCAP1, the potential of their co-presence with respect to GC1 inhibition was explicitly probed. We thus monitored the effects of RD3 on the Ca^{2+}-dependent regulation of GC1 by both GCAP1 variants starting form the case of high and low Ca^{2+} levels, corresponding to dark-adapted and illuminated cells, respectively (Fig. 6A). As expected, the presence of RD3 significantly diminished the rate of cGMP synthesis under activating conditions in the presence of WT-GCAP1 (p-value = 1.62 ×10^{-5}, Table ST2), and under both activating and inhibiting conditions in the presence of E111V-GCAP1 (p-value = 1.30 ×10^{-4} and 7.16 ×10^{-5}, respectively, Table ST2). Notably, though, in the presence of RD3, E111V-GCAP1 exhibited a persistent activation in the presence of Ca^{2+},

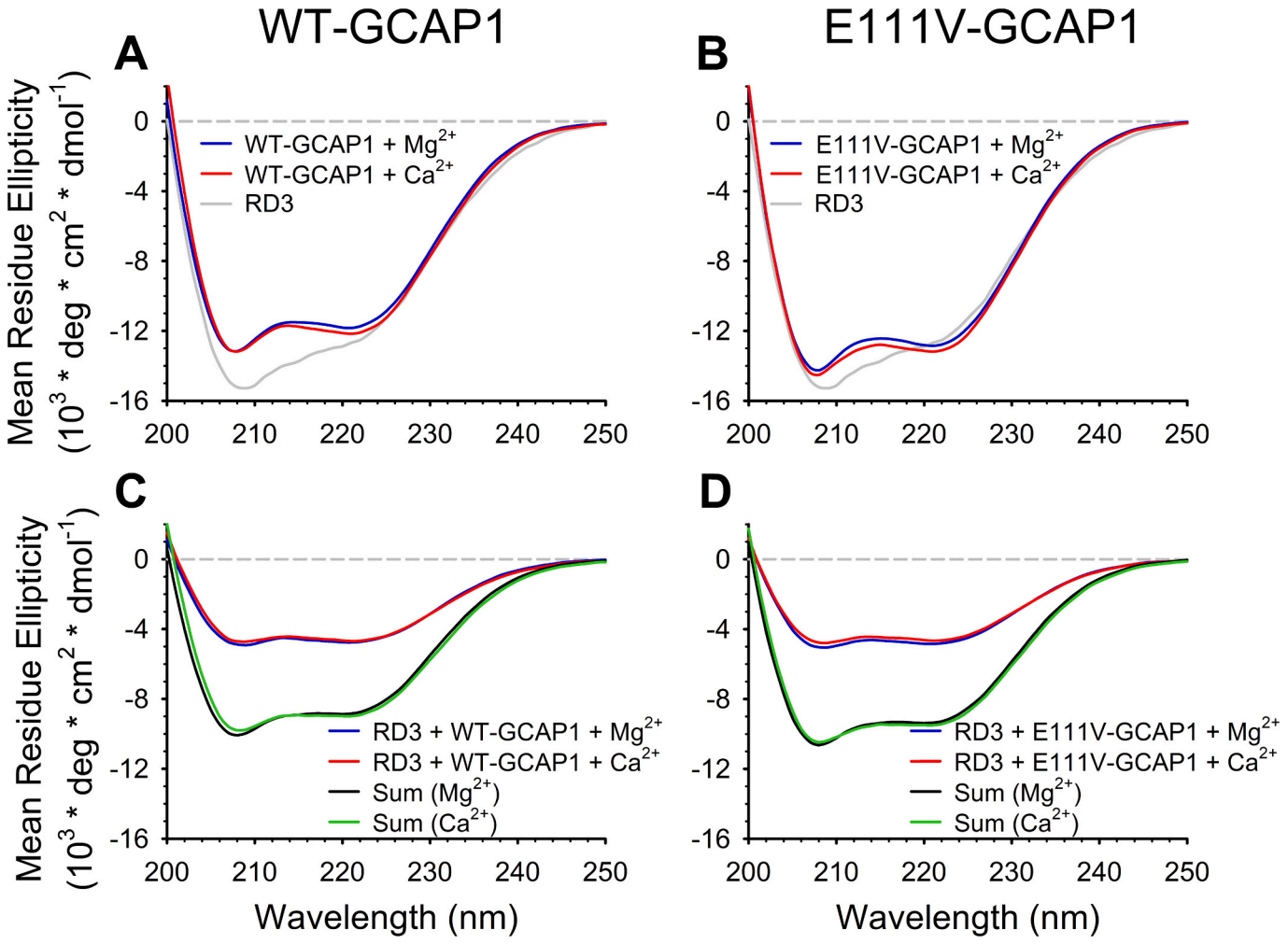

Fig. 4. Effects of RD3 interaction and ion binding on the secondary structure of GCAP1 variants. Far UV CD spectra of: (A) 10 μM RD3 (grey) in the presence 300 μM EGTA, 10 μM WT-GCAP1 in the presence 300 μM EGTA and 1 mM Mg^{2+} (blue) and upon addition of 600 μM Ca^{2+} (300 μM free Ca^{2+}, red); (B) 10 μM RD3 (grey) in the presence 300 μM EGTA, 10 μM E111V-GCAP1 in the presence 300 μM EGTA and 1 mM Mg^{2+} (blue) and upon addition of 600 μM Ca^{2+} (300 μM free Ca^{2+}, red); (D) 10 μM RD3 and 10 μM WT-GCAP1 in the presence 300 μM EGTA and 1 mM Mg^{2+} (blue) and upon addition of 600 μM Ca^{2+} (300 μM free Ca^{2+}, red), sum of the spectra of the isolated molecules in the presence 300 μM EGTA and 1 mM Mg^{2+} (black) and upon addition of 600 μM Ca^{2+} (300 μM free Ca^{2+}, green); (E) 10 μM RD3 and 10 μM E111V-GCAP1 in the presence 300 μM EGTA and 1 mM Mg^{2+} (blue) and upon addition of 600 μM Ca^{2+} (300 μM free Ca^{2+}, red), arithmetic sum of the spectra of the isolated molecules in the presence of 300 μM EGTA (black) and upon addition of 600 μM Ca^{2+} (300 μM free Ca^{2+}, green).

Table 2
Results from CD spectroscopy.

Variant	Δθ/θ (%)[a]	$\theta_{222}/\theta_{208}$
RD3	–	–
Mg^{2+}-bound		
WT-GCAP1	–	0.89
E111V-GCAP1	–	0.89
RD3 + WT-GCAP1	–	0.98
RD3 + E111V-GCAP1	–	0.99
Ca^{2+}-bound		
WT-GCAP1	3.02	0.92
E111V-GCAP1	2.60	0.90
RD3 + WT-GCAP1	1.23	0.99
RD3 + E111V-GCAP1	3.44	1.07

[a] Calculated as $(\theta_{222}^{ion}-\theta_{222}^{EGTA})/\theta_{222}^{EGTA}$.

with a cGMP synthesis substantially indistinguishable from that in the absence of Ca^{2+} (p-value = 0.876, Table ST2), indicative of the strong constitutive activation of GC1 induced by the mutant. Interestingly, the incomplete shut-down of the cyclase activity detected for both variants, observed in this study (Fig. 6A) and in previous ones [24,29] might be attributed to the direct interaction of GCAP1 with RD3, an interplay that, as discussed above, is still poorly understood [30].

As mentioned above, the delivery of extra WT-GCAP1 on a background of E111V-GCAP1 was shown to bring the Ca^{2+}-dependent regulation of GC1 closer the physiological Ca^{2+}-range [32]; to test any synergistic effect in the presence of a potent GC1 inhibitor, we monitored the effects of RD3 on GC1 regulation in the presence of GCAP1 variants at a stoichiometric ratio WT:E111V of 3:1. Remarkably, RD3 was found to almost totally revert the molecular phenotype of the GC1-GCAP1 machinery to that of the WT (Fig. 6B), with an IC_{50} shifting from (8.49 ± 6.05) μM to (0.29 ± 0.05) μM (Table 3), thus comparable to that of the WT both in the absence (0.32 ± 0.02 μM) and in the presence of RD3 (0.22 ± 0.01 μM, Table 3). A similar conclusion could be drawn as to the cooperativity of the GC1's Ca^{2+}-regulation, as displayed by the Hill coefficient switching from 0.68 ± 0.28 in the absence of RD3 to 2.24 ± 0.94 in its presence (Table 3), again very close to the values exhibited by the WT under the same conditions (2.14 ± 0.27 and 2.23 ± 0.28, respectively). Remarkably, RD3 substantially moderated the aberrant cGMP synthesis instigated by the E111V-GCAP1 mutation especially

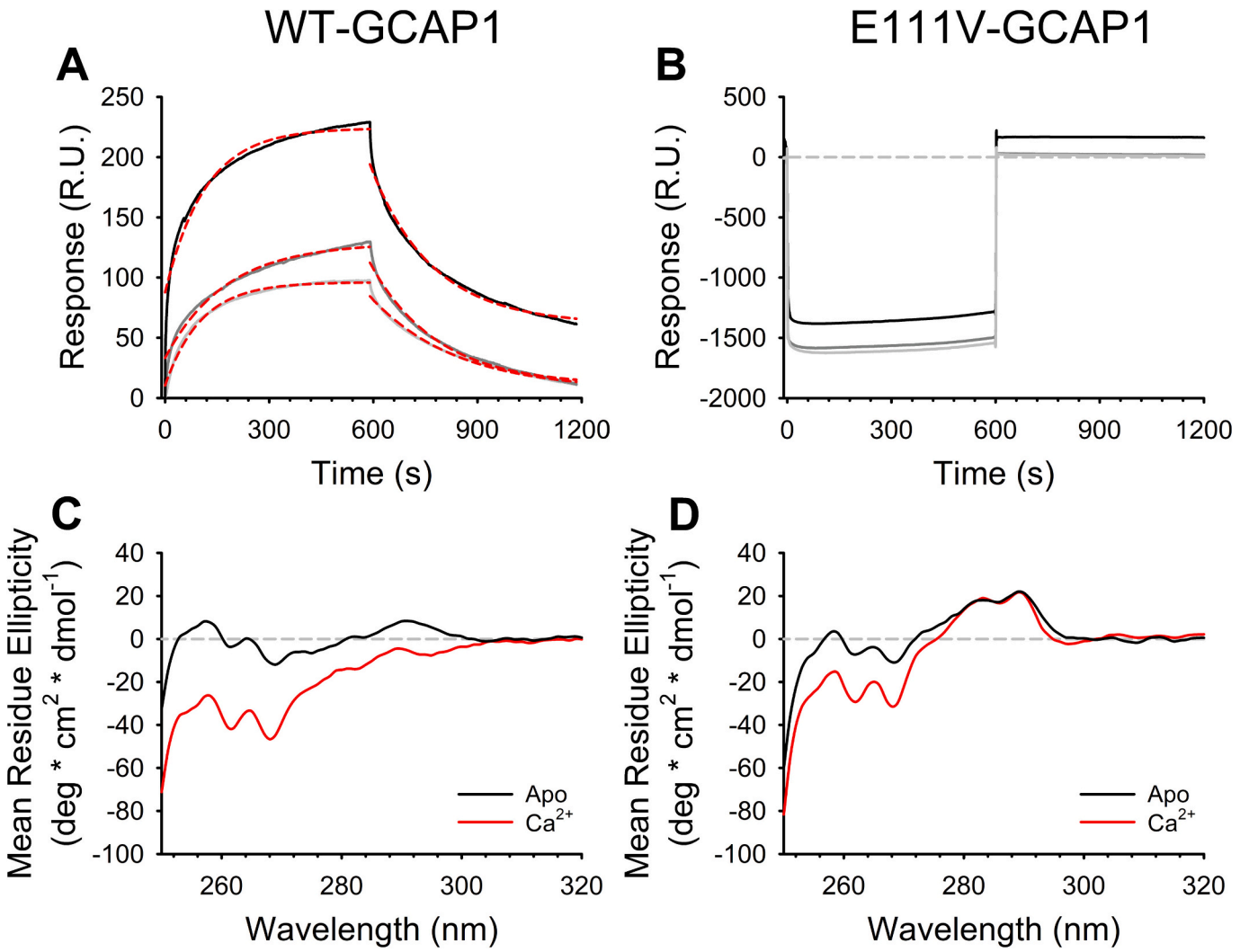

Fig. 5. Interaction between RD3 and GCAP1 variants monitored by surface plasmon resonance and conformational changes occurring in GCAP1 variants upon Ca^{2+}-binding monitored by near UV CD spectroscopy. Representative sensorgrams of A) WT- and B) E111V-GCAP1 injected at 1 μM (light grey), 2 μM (dark grey), and 5 μM (black) over immobilized RD3 using 10 mM HEPES, 150 mM NaCl, 300 μM Ca^{2+}, 0.005 % Tween 20, pH 7.4 as running buffer, with 600 s association and dissociation times, together with the fitting curves (red dashed lines) which allowed the estimation of both rate constants. Near UV CD spectra of ~40 μM C) WT- and D) E111V-GCAP1 in the presence of 500 μM EGTA (black) and after addition of 1 mM Ca^{2+}, leading to 500 μM free Ca^{2+} (red).

Table 3
Results from enzymatic assays.

	Variant	IC_{50}[a] (μM)	h[b]	EC_{50}[c] (μM)	X-fold[d]
	WT[e]	0.32 ± 0.02	2.14 ± 0.27	1.88 ± 0.22	26
- RD3	E111V[e]	20.2 ± 7.6	0.60 ± 0.38	1.55 ± 0.21	1.1
	3xWT/E111V	8.49 ± 6.05	0.68 ± 0.28	–	3.3
	WT	0.22 ± 0.01	2.23 ± 0.28	6.36 ± 1.17	14.4
+ RD3	E111V	118 ± 44.8	0.67 ± 0.95	5.62 ± 1.61	0.76
	3xWT/E111V	0.29 ± 0.05	2.24 ± 0.94	–	4.6

Data are reported as mean ± standard deviation of three technical replicates.
[a] Human GC1 activity as a function of free [Ca^{2+}] in the presence of 5 μM GCAP1 variants and 200 nM RD3.
[b] Hill coefficient.
[c] GCAP1 concentration at which GC1 activity is half-maximal.
[d] Fold change in cGMP production calculated as (GC_{max} - GC_{min})/GC_{min}.
[e] Data from [33].

when complemented with an excess of the WT form (Fig. 6, Table 3).

According to previous results, RD3 may inhibit GC1 activation via two different, but not mutually exclusive, mechanisms, namely: i) RD3 binds GC1 [30] and acts as a competitive inhibitor of GCAP1, thus implying a shared interaction interface on GC1; and ii) the interaction between GCAP1 and RD3 [30] prevents GCAP1 from regulating GC1. Data shown in Fig. 6A might indeed suggest that RD3 acts as a competitive inhibitor of GC1 by sharing the same binding site with GCAP1. However, the Ca^{2+}-dependent regulation of GC1 activity shown in Fig. 6B suggests a more complex mechanism, which might imply a dynamic interaction between GCAP1, RD3 and GC1, as previously suggested by *Zulliger et al.* [30]. Indeed, our SPR data suggest that RD3 binds WT-GCAP1, but not the E111V variant. The hypothesis that RD3 binds preferentially to E111V-GCAP1 preventing it from activating GC1 according to a purely competitive model therefore seems implausible. Since the EC_{50} values for GC1 activation by GCAP1 are essentially the same for the WT and E111V variants (Table 3), a molecular scenario compatible with the Ca^{2+}-dependent regulation of GC1 observed in Fig. 6B is the following. If realized in the photoreceptor outer segment, the direct interaction between WT-GCAP1 and RD3 would restore the physiological regulation of the GC1-GCAP1 complex in the presence of the E111V-GCAP1 variant by strengthening the assembly of the WT-GCAP1-RD3-GC1 complex; the E111V mutant, on the other hand, would interact with GC1 without the mediation of RD3. This mechanistic hypothesis builds on a functional interaction between GCAP1,

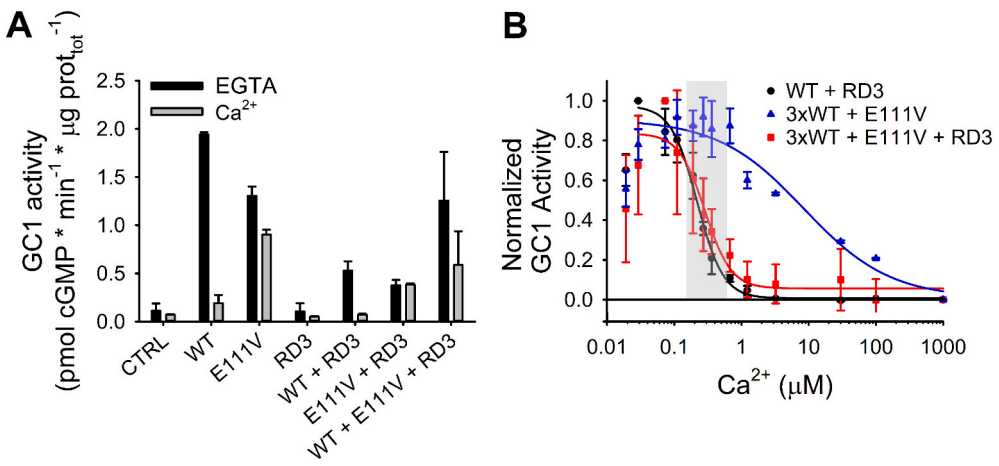

Fig. 6. GC1 regulation by GCAP1 variants in the absence and in the presence of 200 nM RD3. (A) GC1 activity was measured in the presence of 5 μM WT-GCAP1, 5 μM E111V-GCAP1, 200 nM RD3, 5 μM WT-GCAP1 + 200 nM RD3, 5 μM E111V-GCAP1 + 200 nM RD3, 3.75 μM WT-GCAP1 + 1.25 μM E111V-GCAP1 (5 μM at a stoichiometric ratio of 3 WT-GCAP1: 1 E111V-GCAP1) + 200 nM RD3 and < 19 nM Ca^{2+} (black) or ~30 μM free Ca^{2+} (grey); membranes with no GCAP1 or RD3 were used as control. (B) GC1 activity as a function of [Ca^{2+}] was measured in the presence of 5 μM WT-GCAP1 + 200 nM RD3 (black circles), 3.75 μM WT-GCAP1 + 1.25 μM E111V-GCAP1 (blue triangles), and 3.75 μM WT-GCAP1 + 1.25 μM E111V-GCAP1 + 200 nM RD3 (red squares). Normalized GC1 activity was fitted to a 4-parameter Hill sigmoid, the grey box indicates the physiological Ca^{2+} range in photoreceptors (150–600 nM). Data are presented as average ± standard deviation of three technical replicates.

RD3 and GC at the level of the endoplasmic reticulum, which has been postulated to be essential for the cellular localization of GC1, and whose perturbation has been associated with Leber Congenital Amaurosis −1 [30]. Our experimental conditions reproduce the co-presence of all proteins (GC1, RD3, WT-GCAP1 and E111V-GCAP1) in an environment that mimics the photoreceptor outer segment, and could effectively be achieved by specific protein delivery [32] thus resulting in a valid therapeutic option for CORD. However, further studies unveiling essential factors, such as the stoichiometry of protein-protein interactions as well as the concentration of the proteins involved in human photoreceptors are required to prove the hypothesis and elucidate the specific molecular mechanisms.

4. Conclusions

The comprehensive analysis presented here provides new insights into the supramolecular complexes formed by GCAP1 under both physiological and pathological conditions. We used the E111V-GCAP1 variant as representative of more than twenty COD/CORD associated mutations and investigated the dimerization process of GCAP1, which probably plays a role in the regulation of GC1 enzymatic activity. We found that the point mutation does not significantly alter the GCAP1 dimerization. However, the slight changes in affinity detected for E111V-GCAP1 homodimers in the presence of Ca^{2+} suggests that even slight perturbations of the GCAP1 monomer/dimer equilibrium may result in severe dysregulation of GC1, although the dimerization process occurs in a similar manner in structural terms. It remains essential, however, to determine the three-dimensional structure of the GC1-GCAP1 complex and to assess the correct stoichiometry of the interaction, since *per se*, GCAP1 could be predominantly monomeric in the absence of the target. We also explored the influence of RD3 in co-presence with WT- and E111V-GCAP1 on GC1 activity. Enzymatic assays revealed the ability of RD3 to mitigate the aberrant cGMP synthesis caused by the E111V mutation, especially when combined with an excess of WT-GCAP1. This suggests a potential role for RD3 in restoring near-physiological levels of GC1 activity in vitro, thus contributing to the restoration of the disrupted Ca^{2+} and cGMP homeostasis in photoreceptor pathophysiology associated with the E111V mutation. This is particularly interesting in light of our recent findings [33] that support a possible role for protein delivery to the retina (via eye-drops [48] or intravitreal injections [49], the routes used to deliver nerve growth factors) to modulate the phototransduction cascade and virtually counterbalance the constitutive activation of IRD-associated GCAP1 variants.

CRediT authorship contribution statement

Amedeo Biasi: Writing – original draft, Software, Methodology, Investigation. **Valerio Marino:** Writing – review & editing, Formal analysis, Data curation. **Giuditta Dal Cortivo:** Visualization, Investigation. **Daniele Dell'Orco:** Writing – review & editing, Writing – original draft, Supervision, Funding acquisition, Conceptualization.

Declaration of competing interest

The authors declare that they have no known competing financial interests or personal relationships that could have appeared to influence the work reported in this paper.

Acknowledgments

The Centro Piattaforme Tecnologiche of the University of Verona is acknowledged for providing access to the computational and spectroscopic platforms. This study was supported by a grant from the Velux Stiftung (Project No. 1410) and by the Next Generation EU/Ministry of University and Research project: "A multiscale integrated approach to the study of the nervous system in health and disease (MNESYS)", CUP B33C22001060002, PE00000006 missione 4, componente 2, investimento 1.3. Excellent technical assistance by Silvia Bianconi is gratefully acknowledged.

Appendix A. Supplementary data

Supplementary data to this article can be found online at https://doi.org/10.1016/j.ijbiomac.2024.135068.

References

[1] K.-W. Koch, D. Dell'Orco, Protein and signaling networks in vertebrate photoreceptor cells, Front. Mol. Neurosci. 8 (2015).
[2] J.I. Korenbrot, Speed, sensitivity, and stability of the light response in rod and cone photoreceptors: facts and models, Prog. Retin. Eye Res. 31 (5) (2012) 442–466.

[3] J.B. Ames, Dimerization of neuronal calcium sensor proteins, Front. Mol. Neurosci. 11 (2018).
[4] A. Dizhoor, The human photoreceptor membrane guanylyl cyclase, RetGC, is present in outer segments and is regulated by calcium and a soluble activator, Neuron 12 (6) (1994) 1345–1352.
[5] D.G. Lowe, A.M. Dizhoor, K. Liu, Q. Gu, M. Spencer, R. Laura, L. Lu, J.B. Hurley, Cloning and expression of a second photoreceptor-specific membrane retina guanylyl cyclase (RetGC), RetGC-2, Proc. Natl. Acad. Sci. 92 (12) (1995) 5535–5539.
[6] I.V. Peshenko, E.V. Olshevskaya, A.B. Savchenko, S. Karan, K. Palczewski, W. Baehr, A.M. Dizhoor, Enzymatic properties and regulation of the native isozymes of retinal membrane guanylyl cyclase (RetGC) from mouse photoreceptors, Biochemistry 50 (25) (2011) 5590–5600.
[7] A. Biasi, V. Marino, G. Dal Cortivo, P.E. Maltese, A.M. Modarelli, M. Bertelli, L. Colombo, D. Dell'Orco, A novel GUCA1A variant associated with cone dystrophy alters cGMP signaling in photoreceptors by strongly interacting with and hyperactivating retinal guanylate cyclase, Int. J. Mol. Sci. 22 (19) (2021) 10809.
[8] G. Dal Cortivo, V. Marino, F. Bonì, M. Milani, D. Dell'Orco, Missense mutations affecting Ca2+−coordination in GCAP1 lead to cone-rod dystrophies by altering protein structural and functional properties, Biochimica et Biophysica Acta (BBA) - Molecular Cell Research 1867 (10) (2020) 118794.
[9] D. Dell'Orco, P. Behnen, S. Linse, K.-W. Koch, Calcium binding, structural stability and guanylate cyclase activation in GCAP1 variants associated with human cone dystrophy, Cell. Mol. Life Sci. 67 (6) (2010) 973–984.
[10] A.M. Dizhoor, S.G. Boikov, E.V. Olshevskaya, Constitutive activation of photoreceptor guanylate cyclase by Y99C mutant of GCAP-1, J. Biol. Chem. 273 (28) (1998) 17311–17314.
[11] L. Jiang, D. Wheaton, G. Bereta, K. Zhang, K. Palczewski, D.G. Birch, W. Baehr, A novel GCAP1(N104K) mutation in EF-hand 3 (EF3) linked to autosomal dominant cone dystrophy, Vision Res. 48 (23–24) (2008) 2425–2432.
[12] K. Kamenarova, M. Corton, B. García-Sandoval, P. Fernández-San Jose, V. Panchev, A. Ávila-Fernández, M.I. López-Molina, C. Chakarova, C. Ayuso, S.S. Bhattacharya, Novel GUCA1A mutations suggesting possible mechanisms of pathogenesis in cone, cone-rod, and macular dystrophy patients, Biomed. Res. Int. 2013 (2013) 1–15.
[13] V.B.D. Kitiratschky, P. Behnen, U. Kellner, J.R. Heckenlively, E. Zrenner, H. Jägle, S. Kohl, B. Wissinger, K.-W. Koch, Mutations in the GUCA1A gene involved in hereditary cone dystrophies impair calcium-mediated regulation of guanylate cyclase, Hum. Mutat. 30 (8) (2009) E782–E796.
[14] V. Marino, G. Dal Cortivo, E. Oppici, P.E. Maltese, F. D'Esposito, E. Manara, L. Ziccardi, B. Falsini, A. Magli, M. Bertelli, D. Dell'Orco, A novel p., (Glu111Val) missense mutation in GUCA1A associated with cone-rod dystrophy leads to impaired calcium sensing and perturbed second messenger homeostasis in photoreceptors, Hum. Mol. Genet. 27 (24) (2018) 4204–4217.
[15] V. Marino, A. Scholten, K.-W. Koch, D. Dell'Orco, Two retinal dystrophy-associated missense mutations in GUCA1A with distinct molecular properties result in a similar aberrant regulation of the retinal guanylate cyclase, Hum. Mol. Genet. 24 (23) (2015) 6653–6666.
[16] K.M. Nishiguchi, I. Sokal, L. Yang, N. Roychowdhury, K. Palczewski, E.L. Berson, T. P. Dryja, W. Baehr, A novel mutation (I143NT) in guanylate cyclase-activating protein 1 (GCAP1) associated with autosomal dominant cone degeneration, Investigative Opthalmology & Visual Science 45 (11) (2004) 3863.
[17] P. Behnen, D. Dell'Orco, K.-W. Koch, Involvement of the calcium sensor GCAP1 in hereditary cone dystrophies, Biol. Chem. 391 (6) (2010).
[18] F. Bonì, V. Marino, C. Bidoia, E. Mastrangelo, A. Barbiroli, D. Dell'Orco, M. Milani, Modulation of guanylate cyclase activating protein 1 (GCAP1) dimeric assembly by Ca2+ or Mg2+: hints to understand protein activity, Biomolecules 10 (10) (2020) 1408.
[19] E.A. Permyakov, S. Lim, G. Roseman, I. Peshenko, G. Manchala, D. Cudia, A. M. Dizhoor, G. Millhauser, J.B. Ames, Retinal guanylyl cyclase activating protein 1 forms a functional dimer, PloS One 13 (3) (2018) e0193947.
[20] S. Lim, I.V. Peshenko, E.V. Olshevskaya, A.M. Dizhoor, J.B. Ames, Structure of guanylyl cyclase activator protein 1 (GCAP1) mutant V77E in a Ca2+−free/Mg2 +−bound activator state, J. Biol. Chem. 291 (9) (2016) 4429–4441.
[21] S. Lim, G. Roseman, I. Peshenko, G. Manchala, D. Cudia, A.M. Dizhoor, G. Millhauser, J.B. Ames, Retinal guanylyl cyclase activating protein 1 forms a functional dimer, PloS One 13 (3) (2018) e0193947.
[22] L.L. Molday, H. Djajadi, P. Yan, L. Szczygiel, S.L. Boye, V.A. Chiodo, K. Gregory-Evans, M.V. Sarunic, W.W. Hauswirth, R.S. Molday, RD3 gene delivery restores guanylate cyclase localization and rescues photoreceptors in the Rd3 mouse model of Leber congenital amaurosis 12, Hum. Mol. Genet. 22 (19) (2013) 3894–3905.
[23] I.V. Peshenko, E.V. Olshevskaya, A.M. Dizhoor, Functional study and mapping sites for interaction with the target enzyme in retinal degeneration 3 (RD3) protein, J. Biol. Chem. 291 (37) (2016) 19713–19723.
[24] I.V. Peshenko, E.V. Olshevskaya, S. Azadi, L.L. Molday, R.S. Molday, A.M. Dizhoor, Retinal degeneration 3 (RD3) protein inhibits catalytic activity of retinal membrane guanylyl cyclase (RetGC) and its stimulation by activating proteins, Biochemistry 50 (44) (2011) 9511–9519.
[25] A.M. Dizhoor, I.V. Peshenko, Regulation of retinal membrane guanylyl cyclase (RetGC) by negative calcium feedback and RD3 protein, Pflugers Arch. - Eur. J. Physiol. 473 (9) (2021) 1393–1410.
[26] J.S. Friedman, B. Chang, C. Kannabiran, C. Chakarova, H.P. Singh, S. Jalali, N. L. Hawes, K. Branham, M. Othman, E. Filippova, D.A. Thompson, A.R. Webster, S. Andréasson, S.G. Jacobson, S.S. Bhattacharya, J.R. Heckenlively, A. Swaroop, Premature truncation of a novel protein, RD3, exhibiting subnuclear localization is associated with retinal degeneration, Am. J. Hum. Genet. 79 (6) (2006) 1059–1070.
[27] A.M. Dizhoor, E.V. Olshevskaya, I.V. Peshenko, Retinal degeneration-3 protein promotes photoreceptor survival by suppressing activation of guanylyl cyclase rather than accelerating GMP recycling, J. Biol. Chem. 296 (2021) 100362.
[28] S. Azadi, L.L. Molday, R.S. Molday, RD3, the protein associated with Leber congenital amaurosis type 12, is required for guanylate cyclase trafficking in photoreceptor cells, Proc. Natl. Acad. Sci. 107 (49) (2010) 21158–21163.
[29] H. Wimberg, U. Janssen-Bienhold, K.-W. Koch, Control of the nucleotide cycle in photoreceptor cell extracts by retinal degeneration protein 3, Front. Mol. Neurosci. 11 (2018).
[30] R. Zulliger, M.I. Naash, R.V.S. Rajala, R.S. Molday, S. Azadi, Impaired association of retinal degeneration-3 with guanylate Cyclase-1 and guanylate cyclase-activating protein-1 leads to leber congenital Amaurosis-1, J. Biol. Chem. 290 (6) (2015) 3488–3499.
[31] I.V. Peshenko, A.M. Dizhoor, Two clusters of surface-exposed amino acid residues enable high-affinity binding of retinal degeneration-3 (RD3) protein to retinal guanylyl cyclase, J. Biol. Chem. 295 (31) (2020) 10781–10793.
[32] D. Dell'Orco, G. Dal Cortivo, Normal GCAPs partly compensate for altered cGMP signaling in retinal dystrophies associated with mutations in GUCA1A, Sci. Rep. 9 (1) (2019).
[33] S. Asteriti, V. Marino, A. Avesani, A. Biasi, G. Dal Cortivo, L. Cangiano, D. Dell'Orco, Recombinant protein delivery enables modulation of the phototransduction cascade in mouse retina, Cell. Mol. Life Sci. 80 (12) (2023).
[34] J.-Y. Hwang, K.-W. Koch, Calcium- and Myristoyl-dependent properties of guanylate cyclase-activating Protein-1 and Protein-2, Biochemistry 41 (43) (2002) 13021–13028.
[35] M. Bradford, A rapid and sensitive method for the quantitation of microgram quantities of protein utilizing the principle of protein-dye binding, Anal. Biochem. 72 (1–2) (1976) 248–254.
[36] R. Stephen, G. Bereta, M. Golczak, K. Palczewski, M.C. Sousa, Stabilizing function for myristoyl group revealed by the crystal structure of a neuronal calcium sensor, guanylate cyclase-activating protein 1, Structure 15 (11) (2007) 1392–1402.
[37] V. Marino, S. Sulmann, K.-W. Koch, D. Dell'Orco, Structural effects of Mg2+ on the regulatory states of three neuronal calcium sensors operating in vertebrate phototransduction, Biochimica et Biophysica Acta (BBA) – Molecular Cell Res. 1853 (9) (2015) 2055–2065.
[38] V. Marino, D. Dell'Orco, Allosteric communication pathways routed by Ca2+/Mg2 + exchange in GCAP1 selectively switch target regulation modes, Sci. Rep. 6 (1) (2016).
[39] I.V. Peshenko, Q. Yu, S. Lim, D. Cudia, A.M. Dizhoor, J.B. Ames, Retinal degeneration 3 (RD3) protein, a retinal guanylyl cyclase regulator, forms a monomeric and elongated four-helix bundle, J. Biol. Chem. 294 (7) (2019) 2318–2328.
[40] M.J. Abraham, T. Murtola, R. Schulz, S. Páll, J.C. Smith, B. Hess, E. Lindahl, GROMACS: high performance molecular simulations through multi-level parallelism from laptops to supercomputers, SoftwareX 1-2 (2015) 19–25.
[41] J. Huang, S. Rauscher, G. Nawrocki, T. Ran, M. Feig, B.L. de Groot, H. Grubmüller, A.D. MacKerell, CHARMM36m: an improved force field for folded and intrinsically disordered proteins, Nat. Methods 14 (1) (2016) 71–73.
[42] O. Keskin, B.G. Pierce, Y. Hourai, Z. Weng, Accelerating protein docking in ZDOCK using an advanced 3D convolution library, PloS One 6 (9) (2011) e24657.
[43] D. Dell'Orco, P.G. De Benedetti, F. Fanelli, In silico screening of mutational effects on enzyme-proteic inhibitor affinity: a docking-based approach, BMC Struct. Biol. 7 (1) (2007).
[44] D. Dell'Orco, Fast predictions of thermodynamics and kinetics of protein–protein recognition from structures: from molecular design to systems biology, Mol. Biosyst. 5 (4) (2009) 323.
[45] J.B. Ames, Structural basis of retinal membrane guanylate cyclase regulation by GCAP1 and RD3, Front. Mol. Neurosci. 15 (2022).
[46] J.Y. Hwang, C. Lange, A. Helten, D. Höppner-Heitmann, T. Duda, R.K. Sharma, K. W. Koch, Regulatory modes of rod outer segment membrane guanylate cyclase differ in catalytic efficiency and Ca2+−sensitivity, Eur. J. Biochem. 270 (18) (2003) 3814–3821.
[47] Y. Chen, A.U. Bräuer, K.-W. Koch, Retinal degeneration protein 3 controls membrane guanylate cyclase activities in brain tissue, Frontiers in Molecular Neuroscience 15 (2022).
[48] B. Falsini, G. Iarossi, A. Chiaretti, A. Ruggiero, L. Manni, L. Galli-Resta, G. Corbo, E. Abed, NGF eye-drops topical administration in patients with retinitis pigmentosa, a pilot study, J. Transl. Med. 14 (1) (2016).
[49] S. Barnes, L. Domenici, N. Origlia, B. Falsini, E. Cerri, D. Barloscio, C. Fabiani, M. Sansò, L. Giovannini, Rescue of Retinal Function by BDNF in a mouse model of Glaucoma, PloS One 9 (12) (2014) e115579.